Characterizing open and non-uniform vertical heat sources: towards the identification of real vertical cracks in vibrothermography experiments

A. Castelo [a], A. Mendioroz*[a], R. Celorrio [b], A. Salazar [a]
P. López de Uralde [c], I. Gorosmendi [c], E. Gorostegui-Colinas[c]

[a]Departamento de Física Aplicada I, Escuela de Ingeniería de Bilbao, Universidad del País Vasco UPV/EHU, Plaza Ingeniero Torres Quevedo 1, 48013 Bilbao, Spain; [b]Departamento de Matemática Aplicada, EINA/IUMA, Universidad de Zaragoza, Campus Río Ebro, Edificio Torres Quevedo, 50018 Zaragoza, Spain; [c]IK4-Lortek Control and Evaluation Department, Arranomendia kalea 4A 20240 Ordizia, Spain

ABSTRACT

Lock-in vibrothermography is used to characterize vertical kissing and open cracks in metals. In this technique the crack heats up during ultrasound excitation due mainly to friction between the defect's faces. We have solved the inverse problem, consisting in determining the heat source distribution produced at cracks under amplitude modulated ultrasound excitation, which is an ill-posed inverse problem. As a consequence the minimization of the residual is unstable. We have stabilized the algorithm introducing a penalty term based on Total Variation functional. In the inversion, we combine amplitude and phase surface temperature data obtained at several modulation frequencies. Inversions of synthetic data with added noise indicate that compact heat sources are characterized accurately and that the particular upper contours can be retrieved for shallow heat sources. The overall shape of open and homogeneous semicircular strip-shaped heat sources representing open half-penny cracks can also be retrieved but the reconstruction of the deeper end of the heat source loses contrast. Angle-, radius- and depth-dependent inhomogeneous heat flux distributions within these semicircular strips can also be qualitatively characterized. Reconstructions of experimental data taken on samples containing calibrated heat sources confirm the predictions from reconstructions of synthetic data. We also present inversions of experimental data obtained from a real welded Inconel 718 specimen. The results are in good qualitative agreement with the results of liquids penetrants testing.

Keywords: vibrothermography, nondestructive evaluation, infrared thermography, defect characterization, inverse problem.

1. INTRODUCTION

Ultrasound excited thermography also called vibrothermography, sonic infrared (IR) or thermosonics, is a thermographic nondestructive testing technique that has been successfully applied to detect defects such as corrosion [1] and cracks [2,3] in metallic plates and ceramic coatings [4] and delaminations and disbonds in composite structures [5-7]. In vibrothermography, the specimen is excited by high amplitude ultrasounds. If the material is not viscoelastic, like metals, under moderate vibration amplitudes, mechanical energy is dissipated as heat at defects, due mainly to friction between defect faces, so the defect turns into a heat source on a cold environment in the presence of ultrasounds. The thermal energy diffuses in the material and reaches the sample surface, so the defect signature is a hot spot on the surface temperature, which can be monitored with an infrared camera. By modulating the amplitude of ultrasounds at a much lower frequency (lock-in vibrothermography [5]), a periodic heat source is induced at the defect, which produces thermal waves. This periodic heat deposition gives rise to an oscillation of the surface temperature at the modulation frequency. The lock-in process filters this component and evaluates the amplitude and phase lag of the temperature oscillation with

*arantza.mendioroz@ehu.eus

respect to the modulation signal at each pixel in the detector.

In previous works, we combined lock-in amplitude and phase images obtained at several modulation frequencies to characterize the geometry and the depth of artificial vertical kissing cracks [8-11]. Strictly speaking, the physical magnitude that can be retrieved from surface temperature distributions is the periodic heat flux responsible for it. In kissing cracks, the crack lips are in contact and heat is likely to be produced all along the crack surface, so characterizing the heat source distribution excited in a vibrothermography experiment is almost equivalent to characterize the crack geometry itself. The determination of the buried heat source distribution that gives rise to the observed surface temperature amplitude and phase thermograms is an ill-posed inverse problem. It is characterized by small variations in the data giving rise to very large differences in the solution. This makes the minimization of the residual, i.e., the square differences between the data and the calculated temperatures very unstable. We developed an inversion algorithm, stabilized with a penalty term based on total variation functional (TV) [12] and we applied it successfully to characterize the geometry of artificial heat sources that represented vertical kissing cracks, buried bellow the sample surface. We focused on cases where heat production is homogeneous in the area occupied by the crack, as this is the easiest to implement in the samples containing calibrated heat sources that we prepare.

As a further step to approach situations arising in experiments with real cracks, in this work we tackle the case open surface breaking cracks, to which vibrothermography is often applied. It has been shown that, in this kind of cracks, heat is usually produced at a given portion of the crack rather than at the full crack surface: at regions where the crack lips are not in contact there is no frictional heating (unless a clapping mode with high enough vibration amplitude is produced by the ultrasound excitation [13]) and, near the crack border, the closure stresses may lock the crack asperities, which also prevents heat production [14]. Accordingly, heat is generally produced at a certain band where crack lips' contact and relative mobility occur simultaneously. Besides, heat is most likely to be produced inhomogeneously, within the stimulated region. We analyze the performance of the algorithm to characterize open and non homogeneous heat source distributions representing open surface breaking cracks excited by lock-in vibrothermography, as opposed to the closed and compact heat sources that were considered in previous works. In section 2 we recall the direct surface temperature calculation and the inversion procedure. In section 3 we present inversions of synthetic data with added noise corresponding to compact heat sources of different shapes and half-penny shaped homogeneous and inhomogeneous heat source distributions, representing open surface breaking cracks. Next, in section 4, inversions of experimental data taken on two kinds of samples are presented: samples containing artificial cracks represented by calibrated and homogeneous half-ring heat sources, and a cracked real bare Inconel 718 welded sample. Finally, we summarize and conclude.

2. DIRECT AND INVERSE PROBLEMS

Our approach to characterize inner heat source distributions from lock-in vibrothermography data involves the fitting of the data to the result of a semi-analytical model that describes the propagation of the thermal waves generated at the defect. The treatment is purely thermal, as we leave aside the way in which the mechanical wave induces the heating of the defect. In this section we briefly describe the calculation of the complex surface temperature distribution produced by a modulated vertical heat source and the inversion procedure we have developed to stabilize the minimization of the residual and characterize vertical heat sources.

2.1 Direct problem

The first step to characterize heat sources is to solve the direct problem, i.e., to calculate the surface ($z = 0$) temperature distribution generated by a given heat source distribution, modulated at frequency f ($\omega = 2\pi f$), contained in a plane Π ($x = 0$) perpendicular to the sample surface. The geometry of the problem is depicted in Figure 1.
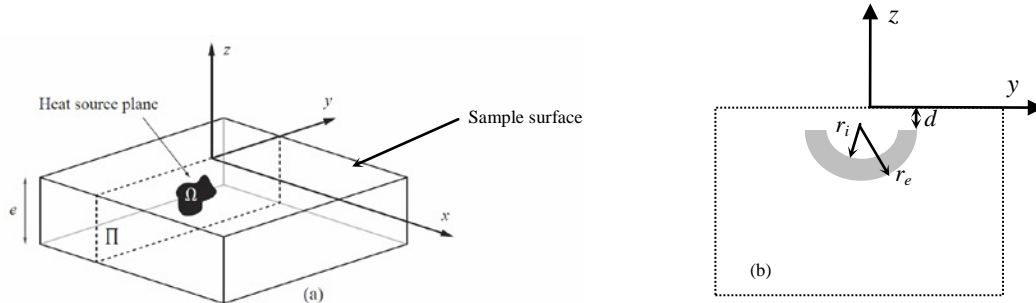

Figure 1. (a) Geometry of the problem. Heat sources of area Ω are contained in plane Π ($x = 0$) and data are taken at the sample surface ($z = 0$). (b) Cross section of a semicircular strip of inner and outer radii r_i and r_e, respectively, buried at a depth d.

The calculation can be easily done by integrating the contribution of point-like, modulated heat sources, covering the desired area Ω, distributed according to a position dependent flux amplitude $Q(\vec{r}\,')$. If the material is semi-infinite, the effect of the surface can be easily accounted for by assuming that heat losses are negligible. In these conditions, the images method can be applied to evaluate the effect of the surface, by considering reflected images of the heat source at the sample surface. The complex surface temperature then writes [8]:

$$T(\vec{r}_{z=0}) = \iint_{\Omega} \frac{Q(\vec{r}\,')}{4\pi K} \frac{e^{-q|\vec{r}-\vec{r}\,'|}}{|\vec{r}-\vec{r}\,'|} dS\,', \qquad \text{with } \vec{r}\,' \in \Pi \ (x = 0)\,, \tag{1}$$

where $q = \sqrt{2\pi i f / D}$ is the thermal wave vector, being D and K the thermal conductivity and diffusivity of the material, respectively. Equation (1) has been evaluated with the thermal properties of AISI 304 stainless steel, the material our samples are made of, to generate synthetic surface temperature data at modulation frequencies $f_k = 0.05, 0.1, 0.2, 0.4, 0.8, 1.6, 3.2, 6.4,$ and 12.8 Hz that will be combined in the inversions presented in section 3.

2.2 Inverse problem

For the inversion, Equation (1) is reformulated by introducing a function $Q_{f_k}(\vec{r})$ that depends on both, position and frequency, to describe the heat source distribution, and integrating over the whole plane Π containing the heat sources, rather than just in area Ω. Function $Q_{f_k}(\vec{r})$ is expressed as the product of two terms, a normalized heat source distribution $Q(\vec{r})$, common to all modulation frequencies, and a set of intensities I_{f_k} that only depend on the modulation frequency:

$$Q_{f_k}(\vec{r}) = I_{f_k} Q(\vec{r})\,. \tag{2}$$

The set on intensities I_{f_k} is introduced in order to be able to increase the ultrasound amplitude at high modulation frequencies where the signal is weaker. The new formulation of the problem is:

$$T_{f_k}(\vec{r}_{z=0}) = \iint_\Pi \frac{Q_{f_k}(\vec{r}\,')}{4\pi K} \frac{e^{-q_{f_k}|\vec{r}-\vec{r}\,'|}}{|\vec{r}-\vec{r}\,'|} dS' = \iint_\Pi \frac{I_{f_k}Q(\vec{r}\,')}{4\pi K} \frac{e^{-q_{f_k}|\vec{r}-\vec{r}\,'|}}{|\vec{r}-\vec{r}\,'|} dS' = A_{f_k}\left[Q_{f_k}\right] = I_{f_k}A_{f_k}\left[Q\right], \quad \text{for } k = 1, \ldots, k_{max}, \qquad (3)$$

where the dependence of the temperatures on frequency has been made explicit T_{f_k}. The integral operator A_{f_k} that maps the heat sources into the surface temperatures is known to give severely ill-posed inverse problems.

The inverse problem, consists in retrieving the heat source distribution that gives rise to a certain surface temperature distribution which, in practice, is affected by noise $T_{f_k}^\delta$, the noise level δ being defined as:

$$\delta^2 = \sum_{k=1}^{k_{max}} \left\| T_{f_k}^\delta - T_{f_k} \right\|^2, \quad \text{with} \quad \|g\|^2 = \iint_{z=0} |g|^2 dS. \qquad (4)$$

Due to the presence of noise, an exact relationship given by Equation (3) does not hold and the problem can be solved in an approximated way by finding the normalized heat source distribution $Q(\vec{r})$ and the set of intensities I_{f_k} that minimize a residual, defined as a the square differences between the data and the calculated temperatures, summed over all modulation frequencies:

$$R^2 = \sum_{k=1}^{k_{max}} \left\| I_{f_k}^\delta A_{f_k} Q^\delta - T_{f_k}^\delta \right\|^2. \qquad (5)$$

The resulting approximated normalized heat source distribution $Q^\delta(\vec{r})$ and intensities $I_{f_k}^\delta$ will be affected by the noise in the data. The ill-posedness of the inverse problem is characterized by very small errors in the data giving rise to arbitrarily large differences in the solution. This makes the minimization of the residual in Equation 5 very unstable.

Our approach to stabilize the inversion consists in introducing a penalty term, based on isotropic total variation functional TV_{ISOT}, defined as [15]:

$$TV_{ISOT}(Q) = \iint_\Pi |\nabla Q| dS \simeq \lim_{j\to\infty} \iint_\Pi \frac{|\nabla Q_j|^2}{\sqrt{\varepsilon + |\nabla Q_{j-1}|^2}} dS = \lim_{j\to\infty} \iint_\Pi \frac{(\partial_y Q_j)^2 + (\partial_z Q_j)^2}{\sqrt{\varepsilon + (\partial_y Q_{j-1})^2 + (\partial_z Q_{j-1})^2}} dS. \qquad (6)$$

As can be seen, TV_{ISOT} is not quadratic, so we approximate it in an iterative way, using lagged fix-point iterations. This iterative process involves the heat source distribution obtained in a previous iteration Q_{j-1}. The first approximation of Q, Q_0, is obtained by regularizing with a penalty term based on zero order Tikhonov functional TK_0 [16], defined as:

$$TK_0(Q) = \iint_\Pi |Q|^2 ds. \qquad (7)$$

The residual to be minimized is now:

$$R_{\vec{\alpha}}^2 = \sum_{k=1}^{k_{max}} \left\| I_{f_k}^{\delta,\vec{\alpha}} A_{f_k} Q^{\delta,\vec{\alpha}} - T_{f_k}^\delta \right\|^2 + \alpha_{TV} TV_{ISOT} + \alpha_{TK_0} TK_0, \quad \text{with } \vec{\alpha} = (\alpha_{TK_0}, \alpha_{TV}). \qquad (8)$$

Each penalty functional is multiplied by a regularization parameter $\vec{\alpha} = (\alpha_{TK_0}, \alpha_{TV})$ that determines the size of the regularization term with respect to the first term on the right hand side of Equation (8), that we will call now the discrepancy term. We start iterations with a rather high value of the regularization parameters and we reduce them in each iteration with different decay factors: α_{TK_0} decays fast, it is reduced by a factor of 0.3 in successive iterations (as mentioned above it is basically used to provide a first approximation of the heat source distribution), and α_{TV} is reduced

by a factor of 0.75. The iterations are stopped when the minimum residue term is found. It is worth mentioning that, solutions recovered even one or two iterations after the minimal residue iteration are observed to be physically meaningful. In some sense, it seems that a second Morozov's discrepancy principle applies to this problem, achieved after the minimizer iteration. In order to simplify and automatize recovered solutions we stop iterations when the minimum discrepancy term is found.

3. INVERSION OF SYNTHETIC DATA

In a previous work [11], we inverted synthetic data to analyze the ability of the algorithm to characterize standard 1 mm^2 heat sources of different geometries, located at different depths below the sample surface. Using Equation 1, we generated surface temperature data at the abovementioned frequencies (between 0.05 and 12.8 Hz) and added 5% noise, uniformly distributed in the whole frequency range. Since the noise in amplitude thermograms is determined by the number of images analyzed in the lock-in process, this is representative of an experiment in which the same number of images is analyzed at all modulation frequencies.

We have further analyzed whether the algorithm is able to determine the particular shape of the heat source. In Figure 3 we present some of the results we have obtained for square, semicircular and triangular heat sources. It is a grey level diagram representing the normalized heat source distribution $Q(\vec{r})$ retrieved in plane Π, perpendicular to the sample surface, white represents the maximum value of 1, and black means absence of heat sources. The real contours are depicted in red. In all cases, surface temperature data were generated by setting a homogeneous flux within the considered area.
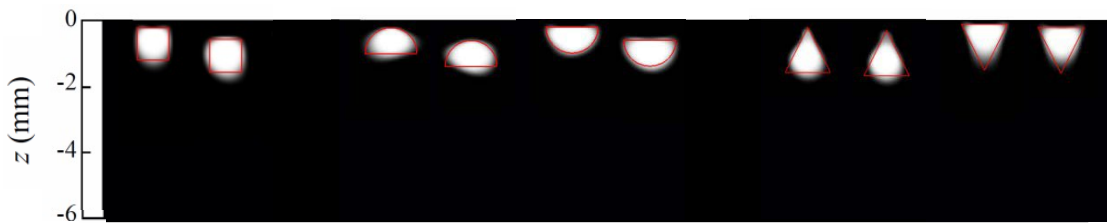

Figure 2. Grey level representation of the retrieved normalized heat source distributions obtained by inverting synthetic data with 5% noise, corresponding to homogeneous (a) square, (b) semicircular and (c) triangular 1 mm^2 heat sources. White is maximum value (1) and black, absence of heat sources. Real contours of the heat sources are depicted in red.

As can be seen, the reconstructions we find for these compact and homogeneous heat sources, representative of kissing cracks are very good. The upper contour is well retrieved only at these shallow depths but we found that all the contours get rounded for deeper heat sources. This rounding effect on the reconstructions is due to the action of TV_{ISOT}, which tends to reduce the contour of the region where the retrieved function has non-zero values and thus delivers round shapes.

As a first step to characterize surface breaking cracks, we have considered kissing surface breaking cracks emitting a homogeneous flux along the crack area. We have chosen half-penny shaped cracks as it is a regular geometry for which Equation 1 can be easily calculated, and that is also usually encountered in real cracks [14]. In Figure 3 we show the reconstructions we have obtained for three different cases, going from a deep and narrow to shallow and elongated geometries. As can be seen, in all cases the heat sources are very well retrieved.
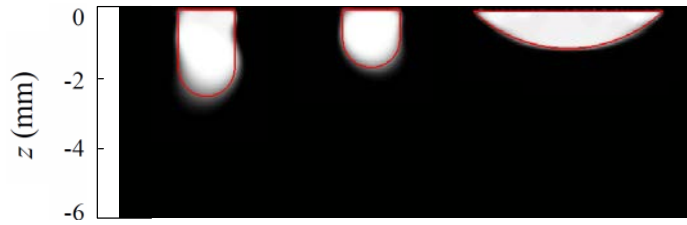
Figure 3. Reconstructions obtained from synthetic data with 5% added noise for half-penny shaped heat sources of different geometries. The data were generated setting a homogeneous flux within the red contours.

On the contrary, when the crack is open, heat is likely to be produced only at a certain contour, as mentioned in the introduction. Next, we have looked at the performance of the algorithm to retrieve contours of a certain width, rather than a compact heat source, like the ones in Figures 2 and 3.

In Figure 4 (a) we show noisy (5%) natural logarithm of amplitude and phase thermograms calculated at 0.2 Hz for a strip heat source of semicircular shape with inner and outer radii $r_i = 1$ mm and $r_e = 1.4$ mm, respectively, buried $d = 0.1$ mm below the surface, and emitting a homogeneous flux. The fitted thermograms are displayed in Figure 4 (b).
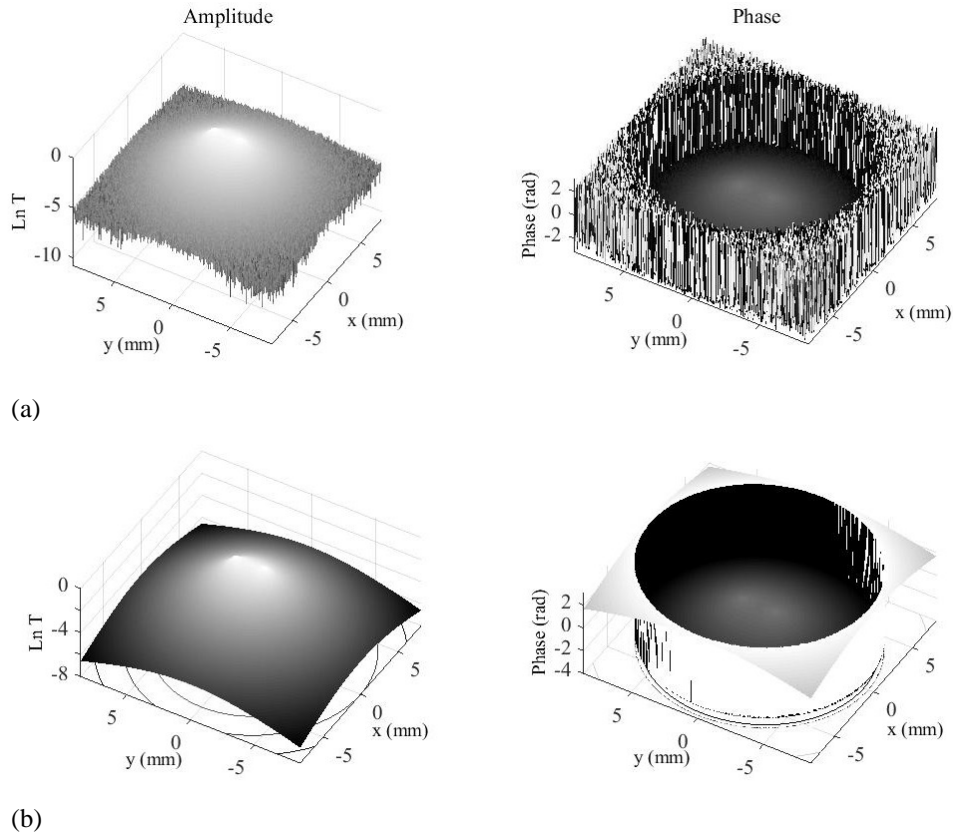

(a)

(b)

Figure 4. (a) Noisy data, natural logarithm of amplitude (left) and phase (right) and (b) fitted thermograms corresponding to a homogeneous semicircular strip of inner and outer radii $r_i = 1$ mm and $r_e = 1.4$ mm, respectively, buried $d = 0.1$ mm below the surface obtained at 0.2 Hz. Data are affected by 5% noise.

The reconstruction is depicted in Figure 5 (right end), together with reconstructions of semicircular strips of smaller outer radii, namely, r_e = 1.16, 1.22, 1.28, and 1.34. As can be seen, the reconstructions are very accurate for the wider strips, but some shadowing effect appears as the width of the strip is decreased: the shallower tips appear brighter and the reconstructed deep central part looks fainter and more diffuse, i.e., some definition is lost at the central deep region.
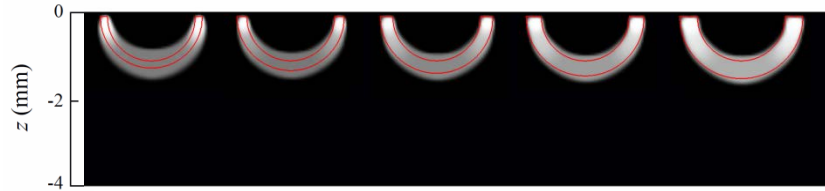

Figure 5. Reconstructions of synthetic data with added 5% noise corresponding to half strips of inner radius r_i = 1 mm and outer radii r_e = 1.16, 1.22, 1.28, 1.34 and 1.4 mm emitting a homogeneous flux. The depth of the upper side is 0.1 mm in all cases.

To further approach experiments performed with real cracks, we have also considered inhomogeneous fluxes within the semicircular strip. We have analyzed three possible cases: flux varying with depth, with angle and with radius. In figure 6 we present the reconstructions we have obtained, together with the heat source distributions that were used to generate the data. The thickness of the strip is 0.4 mm in Figures 6 (a) and (b), but in Figure 6 (c) the thickness has been increased to 0.8 mm. The depth of the upper ends is 0.1 mm in all cases.
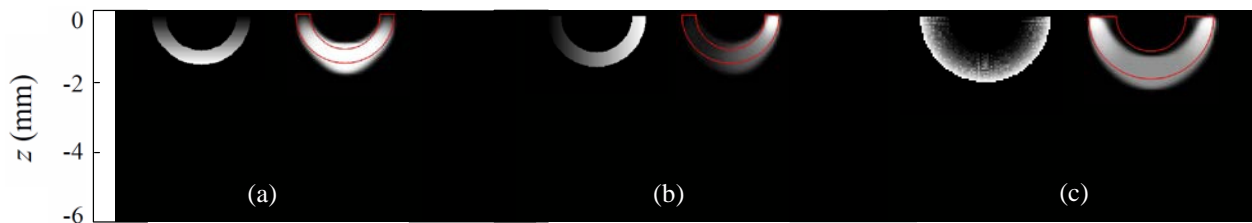

Figure 6. Reconstructions of inhomogeneous semicircular strips from data affected by 5% noise: (a) flux varies with depth, (b) with angle, and (c) with radius. In each case, the figure on the left represents the real heat source distribution from which surface temperature data were generated and the figure on the right is the reconstruction.

As can be seen, reconstructions of heat fluxes varying with depth and with angle are qualitatively well retrieved, whereas the radial dependence of the flux is not reproduced in the reconstruction. Anyway, these results show that TV_{ISOT} can be used to retrieve not only compact heat sources representing kissing cracks, but also these strip shaped heat sources that surround an empty area, representing open cracks. The reconstructions provide quite accurate estimations of the area where heat is generated but the detailed heat source distribution cannot be quantitatively trusted so far.

4. INVERSION OF EXPERIMENTAL DATA

In order to check the ability of the inversion method to characterize open cracks from experimental data, we took data on steel samples containing calibrated heat sources representing open artificial cracks. The configuration is intended to generate a homogeneous flux along the artificial crack surface. Sample preparation was described elsewhere [8]. Basically, it consist in machining two identical AISI 304 stainless steel parts with a flat, well rectified common surface, where thin (38 μm) Cu films are placed to act as calibrated heat sources. Figure 7 shows a sketch of the samples. The

two steel parts with the Cu film in between are attached with screws and the rubbing between the Cu film and the steel parts under the action of the ultrasounds produces the calibrated heat source. The dimensions and depth of the heat source are measured with a stereoscope. In order to prevent any contact between the steel flat surfaces and to guarantee a reasonable homogeneous heat generation in the Cu surfaces, two more Cu films are placed at the back side of the flat surfaces so that the friction produced there does not affect the temperature at the surface where data are taken.
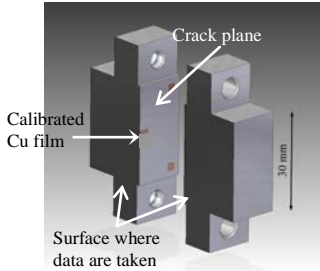

Figure 7. Sketch of the samples containing calibrated vertical heat sources. The temperature is measured at the front surface and the Cu slabs acting as heat sources are pressed between the two halves, perpendicular to the sample surface.

We excite the sample using a UTVis equipment from Edevis. The ultrasound frequency is tunable between 15 and 25 kHz, with a maximum power of 2.2 kW at 20 kHz. We work at an ultrasound frequency of 23 kHz, at which we find the optimum signal in our samples and we modulate the ultrasounds amplitude at frequencies of 0.05, 0.1, 0.2, 0.4, 0.8, 1.6, 3.2, 6.4, and 12.8 Hz. The ultrasound power is kept relatively low (about 25-40 W) in order for the sample to reach the steady state fast and to avoid any damage. In these samples containing artificial cracks we cover the sample surface with a thin layer of black paint to improve the infrared emissivity. The infrared radiation emitted from the surface is captured by an infrared video camera (JADE J550M from Cedip) working in the 3.5 – 5 μm range. It is equipped with a 320 x 240 InSb detector and the NETD is 25 mK. We improve the signal to noise ratio by analyzing about 20000 images using the lock-in technique. The average noise level in amplitude images is then 0.4 mK [17]:

$$\left\langle A_{amp} \right\rangle = 2 \frac{NETD}{\sqrt{N_{images}}} . \tag{9}$$

Running the camera with a half-frame sub-windowing, a frame rate of 320 images per second can be reached, so the full set of 9 frequencies run takes about 10 minutes. We place the camera at the minimum working distance with the optical axis perpendicular to the sample surface, so that the focal plane array images the sample surface without distortion. In these conditions, each pixel in the camera averages the temperature in a 135 μm square side in the sample.

Using this sample, we took data using semicircular and triangular strips of Cu, representing open cracks with homogeneous heat generation within the area under consideration. As an example, in Figure 8 we show experimental natural logarithm of amplitude and phase data corresponding to a semicircular Cu strip of inner radius $r_i = 2$ mm, outer radius $r_e = 3$ mm located at a depth of $d = 0.2$ mm, obtained at 0.2 Hz.
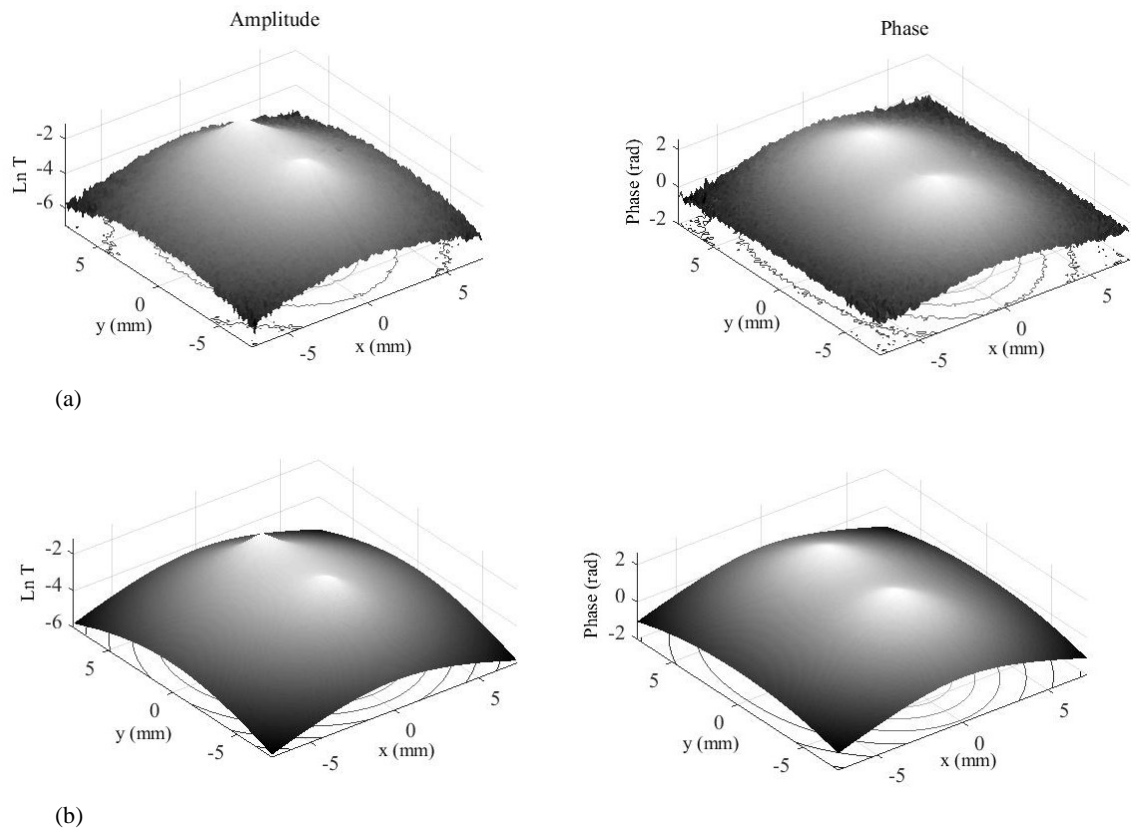
Figure 8. (a) Experimental and (b) fitted natural logarithm of amplitude (left) and phase (right) corresponding to a semicircular Cu strip of inner radius $r_i = 2$ mm, outer radius $r_e = 3$ mm located at a depth of $d = 0.2$ mm, obtained at 0.2 Hz.

The reconstruction is depicted in Figure 9 (a), together with the real contour in red. Figure 9 (b) shows the reconstruction obtained for a triangular Cu slab buried 0.36 mm below the surface and Figure 9 (c) corresponds to a smaller semicircular strip of inner radius $r_i = 1.2$ mm, outer radius $r_e = 2.2$ mm located at a depth of $d = 0.71$ mm.
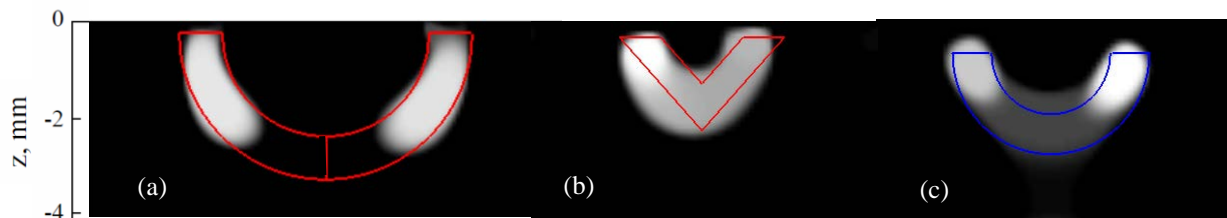

Figure 9. Experimental reconstructions corresponding to (a) a semicircular Cu strip of inner radius $r_i = 2$ mm, outer radius $r_e = 3$ mm located at a depth of $d = 0.2$ mm, (b) a triangular Cu slab buried 0.36 mm below the surface and (c) a semicircular strip of inner radius $r_i = 1.2$ mm, outer radius $r_e = 2.2$ mm located at a depth of $d = 0.71$ mm. Real contours of the Cu slabs in colour.

As can be seen, the shadowing effect is rather pronounced in experimental data, and the reconstruction of the largest semicircle (Figure 9 (a)) miss the contribution of the deeper heat sources. The shape of the reconstruction is rounded in

both cases, due to the effect of TV_{ISOT}, but the depths are well estimated and the reconstructions delimit rather accurately the region where heat is produced.

Finally, we took data on a welded Inconel 718 sample containing real instead of artificial defects. Due to owner requirements, this specimen could not be coated with high emissivity paint, so data were taken on the bare sample, making the test more challenging. Figure 10 (a) shows a visible picture of the test piece. We performed a liquids penetrants testing in the sample to identify surface breaking defects. The result of the test in the area delimited by the red rectangle is depicted in Figure 10 (b). The test produced two indications: a rather visible one, marked with a rectangle in Figure 10 (b) and a secondary fainter indication, surrounded by an ellipse. We performed vibrothermography experiments in this sample exciting it with a frequency sweep within the frequency range of our equipment, from 15 to 25 kHz. In Figure 10 (c) we show the thermogram corresponding to the ultrasound frequency (22.9 kHz) at which we found a clear evidence of the presence of two defects, marked with ellipses. The one on the right coincides with the position of the weak indication in penetrants testing (red ellipse in Figure 10 (b)) and the one on the left did not give any indication in the liquids penetrants testing. These two marked regions in Figure 10 (c) were identified as defects because the signal was dependent on the ultrasound frequency whereas any other feature in the image was static and independent of whether the sample was excited or not. A second ultrasound frequency (24.3 kHz) was also found to excite the defects efficiently.
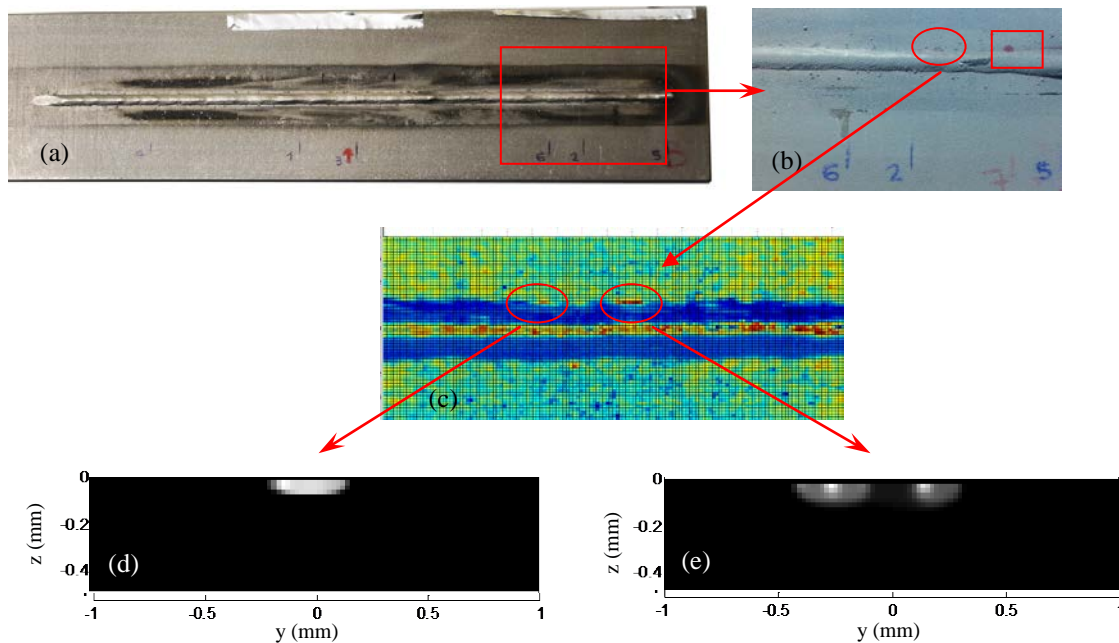

Figure 10. (a) Visible picture of the Inconel 718 welded sample. (b) Zoomed rectangular area depicted in (a) of the result of the liquids penetrants testing. (c) Thermogram in the frequency sweep sequence corresponding to an ultrasound frequency of 22.9 kHz, where the defects are more visible. (d) and (e) Reconstructions of the defects surrounded by ellipses in (c), obtained by exciting the sample at an ultrasound frequency of 22.9 kHz and combining lock-in data at modulation frequencies of 0.1, 0.2, 0.4, and 0.8 Hz.

Exciting the sample at the optimum ultrasound frequency of 22.9 kHz, we took data by modulating the amplitude at frequencies of 0.1, 0.2, 0.4, and 0.8 Hz. The resulting reconstructions from the signals in the marked regions in Figure 10 (c) are shown in Figures 10 (d) and (e). The reconstructions indicate that these are shallow defects, the maximum depth being about 50 and 100 μm, respectively. In the later, two main heat sources are identified in the reconstruction. The shallow reconstruction depicted in Figure 10 (e) is compatible with the faint liquids penetrants testing indication (ellipse

in Figure 10 (b)), pointing out a very small defect volume. The reconstruction of the left hand side crack in Figure 10 (c) is even smaller which could be consistent with the absence of any liquids trace. On the contrary, the stronger indication marked with a rectangle in Figure 10 (b) did not give any signal in the vibrothermography testing. Two reasons could be responsible for this. On the one hand, the larger liquid exuded volume might point out to an open defect, in which case rubbing friction barely takes place. Another possibility is that the ultrasound frequency that activates that defect is outside our frequency range.

5. SUMMARY AND CONCLUSIONS

In this work we apply a stabilized inversion algorithm to characterize open and kissing cracks from lock-in vibrothermography data. In the inversion we combine surface temperature amplitude and phase data obtained at several modulation frequencies. The inversions of synthetic data with added uniform noise indicate that the area and depth of compact heat sources representing kissing cracks can be retrieved accurately and that the algorithm is able to reproduce the particular geometry of the upper contour of shallow heat sources. The ability of the inversion method to characterize semicircular strip-shaped heat sources representing half-penny open cracks has also been checked. The inversions of strips emitting a homogeneous flux indicate that the algorithm is able to retrieve the geometry of the heat source quite accurately for strips wider than 0.3 mm. In thinner strips a shadowing effect is observed in which the shallower side of the heat source is better defined than the deeper region. Finally, data corresponding to inhomogeneous semicircular strips have been inverted, corresponding to depth-, angle- and radius-dependent fluxes. In the first two cases, the reconstructed heat sources are in good qualitative agreement with the real distributions but the retrieved flux is not able to reproduce a radial dependence. The inversion algorithm has also been checked with experimental data taken on samples containing calibrated and homogeneous heat sources with the shape of semicircular strips. The shadowing effect is also encountered when inverting experimental data, especially in cases of large radii, where the lower side of the semicircle is buried deep below the surface. However, the depths and overall areas of shallower heat sources are nicely retrieved. Finally, we inverted experimental data taken on a bare welded Inconel 718 sample. We observed the presence of two defects, the position of one of them coinciding with one indication in the liquids penetrants testing. The weak penetrants testing indication is in good qualitative agreement with the shallow heat source reconstructed from vibrothermography experiments. A larger penetrant testing indication was not found in vibrothermography experiments, probably because it is an open crack that barely produces heat under ultrasounds excitation. A second very small and shallow defect found with vibrothermography did not give any indication in the penetrants testing. Further work is needed to improve the performance of the algorithm to characterize inhomogeneous heat flux distributions.

REFERENCES

[1] Salerno, A., Dillenz, A., Wu, D., Rantala, J., and Busse, G., "Progress in ultrasound excited thermography", Proceedings of the 4th Conference on Quantitative Infrared Thermography, Lodz, Poland, 154-160 (1998).

[2] Montanini, R., Freni, F., and Rossi, G. L., "Quantitative evaluation of hidden defects in cast iron components using ultrasound activated lock-in vibrothermography" Rev. Sci. Instr. **83**, 094902 (8pp) (2012).

[3] Guo, X., and Vavilov, V., "Crack detection in aluminum parts by using ultrasound excited infrared thermography" Infr. Phys. Tech. **61**, 149-156 (2013).

[4] Piau, J. P., Bendada, A., Maldague, X., and Legoux, J.-G., "Nondestructive testing of open microscopic cracks in plasma-sprayed-coatings using ultrasound excited thermography" Nondestr. Test. Eval. **23**, 109-120 (2008).

[5] Rantala, J., Wu, D., and Busse, G., "Amplitude-modulated lock-in vibrothermography for NDE of polymers and composites", Res. Nondestr. Eval. **7**, 215-228 (1995).

[6] Favro, L. D., Han, X., Ouyang, Z., Sun, G., and Thomas, R. L., "Sonic IR imaging of cracks and delaminations" Analitical Sciences **17**, 451-453 (2001).

[7] Barden, T. J., Almond, D. P., Pickering, S. G., Morbidini, M., and Cawley, P., "Detection of impact damage in CFRP composites by thermosonics" Nondestr. Test. Eval. **22**, 71-82 (2007).

[8] Mendioroz, A., Castelo, A., Celorrio, R., and Salazar, A., "Characterization of vertical buried defects using lock-in vibrothermography: I. Direct problem" Meas. Sci. Technol. **24**, 065601 (11pp) (2013).

[9] Celorrio, R., Mendioroz, A., and Salazar, A., "Characterization of vertical buried defects using lock-in vibrothermography: II. Inverse problem" Meas. Sci. Technol. **24**, 065602 (9pp) (2013).

[10] Mendioroz, A., Castelo, A., Celorrio, R., and Salazar, A., "Characterization and spatial resolution of cracks using lock-in vibrothermography" *NDT&E Int.* **66**, 8-15 (2014).

[11] Castelo, A., Mendioroz, A., Celorrio, R., and Salazar, A., "Optimizing the inversion protocol to determine the geometry of vertical cracks from lock-in vibrothermography" J. Nondestr. Eval. **36**, 3 (12pp) (2017).

[12] Brune, C., Sawatzky, A. and Burger, M., "Primal and Dual Bregman Methods with Application to Optical Nanoscopy" Int. J. Comput. Vis. **92**, 211-229 (2011).

[13] Rothenfusser, M. and Homma, C., "Acoustic thermography: vibrational modes of cracks and the mechanism of heat generation" AIP Conf. Proc. **760**, 624-631 (2005).

[14] Renshaw, J., Chen, J. C., Holland, S. D., and Thompson, R. B., "The sources of heat generation in vibrothermography" NDT&E Int **44**, 736-739 (2011).

[15] Brune, C., Sawatzky, A., and Burger, M., "Primal and Dual Bregman Methods with Application to Optical Nanoscopy" Int. J. Comput. Vis. **92**, 211-229 (2011).

[16] Vogel, C, R., Computational Methods for Inverse Problem (Philadelphia, PA: SIAM) (2002).

[17] Breitenstein, O., Warta, W., and Langenkamp, M., Lock-in Thermography: Basics and use for Evaluating Electronic Devices and Materials, Series in Advanced Microelectronics, Springer-Verlag, Berlin Heidelberg (2003).